HHS Public Access

Author manuscript

Vision Res. Author manuscript; available in PMC 2020 May 01.

Published in final edited form as:

Vision Res. 2019 May ; 158: 90–99. doi:10.1016/j.visres.2019.02.009.

Evaluating Seasonal Changes of Cone Photoreceptor Structure in the 13-Lined Ground Squirrel

Benjamin S. Sajdak[1], **Alexander E. Salmon**[1], **Katie M. Litts**[2], **Clive Wells**[3], **Kenneth P. Allen**[4,5], **Alfredo Dubra**[6], **Dana K. Merriman**[7], and **Joseph Carroll**[1,2,8]

[1]Cell Biology, Neurobiology, and Anatomy, Medical College of Wisconsin, Milwaukee, WI, USA

[2]Ophthalmology & Visual Sciences, Medical College of Wisconsin, Milwaukee, WI, USA

[3]Microbiology and Molecular Genetics, Medical College of Wisconsin, Milwaukee, WI, USA

[4]Biomedical Resource Center, Medical College of Wisconsin, Milwaukee, WI, USA

[5]Microbiology and Immunology, Medical College of Wisconsin, Milwaukee, WI, USA

[6]Department of Ophthalmology, Stanford University, Stanford, CA, USA

[7]Biology, University of Wisconsin Oshkosh, Oshkosh, WI, USA

[8]Biophysics, Medical College of Wisconsin, Milwaukee, WI, USA

Abstract

Cone photoreceptors of the 13-lined ground squirrel (13-LGS) undergo reversible structural changes during hibernation, including cone outer segment disc degeneration and inner segment mitochondria depletion. Here, we evaluated cone structure with adaptive optics scanning light ophthalmoscopy (AOSLO) before, during, and after hibernation. Also, intra-animal comparisons of cone structure were made at distinct physiological states (pre-hibernation, torpor, interbout euthermia, and post-hibernation) with AOSLO and transmission electron microscopy. Our results indicate that the 13-LGS cone mosaic is only transiently affected by structural remodeling during hibernation. Outer segment remodeling starts during torpid states during a period of fall transition in room temperature, with more severe structural changes during bouts torpor in cold temperature. Cones return to euthermic-like structure during brief periods of interbout euthermia and recover normal waveguiding properties as soon as 24 hours post-hibernation. Cone structure is visible with split-detector AOSLO thrSoughout hibernation, providing evidence that intact outer segments are not necessary to visualize cones with this technique. Despite the changes to cone structure during hibernation, cone density and packing remained unchanged throughout the seasonal hibernation

Corresponding Author: Joseph Carroll, Department of Ophthalmology & Visual Sciences, Medical College of Wisconsin, 925 N 87th St, Milwaukee, WI 53226-0509, jcarroll@mcw.edu; Phone: (414) 955-2052; Fax: (414) 955-6690.

Disclosures: B.S. Sajdak, none; A.E. Salmon, none; D.K. Merriman, none; K.M. Litts, none; C. Wells, none; K.P. Allen, none; A. Dubra, none; J. Carroll, none

cycle. Pairing non-invasive imaging with ultrastructural assessment may provide insight to the biological origins of cone photoreceptor signals observed with AOSLO.

Keywords

Cone photoreceptors; Ground Squirrel; Adaptive Optics; Hibernation; Electron Microscopy

1. Introduction

The retina is a uniquely accessible neural tissue, and technological advancements allowing *in vivo* assessment of cellular structures *en face* have come a long way since initial success of viewing the cone mosaic using the eye's natural optics (Jagger, 1985; Land and Snyder, 1985; Miller et al., 1996; Wade and Fitzke, 1998). Correction of the eye's monochromatic aberrations with adaptive optics scanning light ophthalmoscopy (AOSLO) results in nearly diffraction-limited imaging of the cone mosaic (Roorda et al., 2002). While cone disorders have been extensively studied non-invasively in patients using AOSLO (Roorda and Duncan, 2015), biological interpretation of cone structure seen with this instrumentation is not well understood. With confocal AOSLO imaging in visually normal human subjects, cones appear as bright or reflective spots. This reflective appearance is often linked to the cone's ability to guide light back to the system's detector (i.e., "waveguiding"), and this reflectivity varies over time (Pallikaris et al., 2003). In patients with cone dystrophies, cones often have reduced or absent waveguiding (Carroll et al., 2008; Song et al., 2015; Sun et al., 2016), though some patients will show spontaneous recovery of cone reflectivity over time (Horton et al., 2015). Some cones can have measurable function in regions of abnormal or absent reflectivity (Bruce et al., 2015; Tu et al., 2017; Wang et al., 2015), suggesting that non-reflective cones may still have some light-capturing structure to provide this function.

The alternative modality of non-confocal split-detection AOSLO can reveal residual cone structure that otherwise appears dim or absent when using only confocal AOSLO (Scoles et al., 2014). Combining confocal AOSLO with split-detection AOSLO to reveal reflective and non-reflective cone structure simultaneously makes this method potentially capable of assessing living cone structure and function at a sub-cellular level. While cone structure seen with split-detection AOSLO is thought to correspond to the cell's inner segment due to a comparable inner diameter when examined with histology (Scoles et al., 2014), it is not known whether an intact outer segment is required for the visualization of cones with split-detection AOSLO. Further, it is not known how changes to cone outer segments alter confocal AOSLO reflectivity. Insight into these questions can be gained from the use of cone-rich animal models. For example, ground squirrel evolution has provided us a natural model of reversible cone degeneration with which to address the interpretation of AOSLO images (Merriman et al., 2016).

The 13-lined ground squirrel (13-LGS; *Ictidomys tridecemlineatus*) has a cone-dominant retina that can be readily imaged with AOSLO (Sajdak et al., 2016). These diurnal rodents hibernate for 5–8 months starting in the fall. Hibernation is a regulated adaptation of metabolic flexibility used by some mammals to survive lengthy periods of limited resources.

This phenomenon is known for its drastic state of suppressed metabolic activity accompanied by whole-body hypothermia, known as torpor, that lasts several days (Andrews, 2007; Staples, 2016). Ground squirrel hibernation is not a single continuous period of metabolic suppression and cold body temperature; instead, it is a cycle that includes a series of torpor bouts with brief periods of increased metabolism and body temperature back to euthermic levels (Figure 1). Each 13-LGS prepares for hibernation during a period of fall transition, in which it experiences varying degrees of heterothermy in room temperature (Russell et al., 2010). Once introduced to ambient cold (4°C), each bout of torpor last about 1–2 weeks, interrupted by energetically costly states of interbout euthermia (IBE, also called interbout arousal) that last about 12–24 hours (Carey et al., 2003; Staples, 2016). Physiological characteristics of torpor in the 13-LGS include reduced body temperature to 2–10°C (compared to 37°C in euthermia) and a heart rate as low as 3–10 beats per minute (compared to 200–300 beats per minute in euthermia) (Andrews, 2007). The hibernation cycle can be reliably monitored within laboratory conditions (Merriman et al., 2012), making it an appealing natural state during which to study tissue resilience to prolonged cold environments and drastically decreased metabolism. While hibernation is commonly used to study unique adaptations in heart, kidney, skeletal muscle, and adipose tissue (Staples, 2016), it is less commonly used to study adaptations of the visual system (Merriman et al., 2016).

During hibernation, 13-LGS cones imaged with transmission electron microscopy (TEM) have been shown to exhibit shortened (potentially absent) outer segments and depleted inner segment mitochondria (Kuwabara, 1975; Remé and Young, 1977); see (Merriman et al., 2016) for a complete review of retinal remodeling in the ground squirrel. Upon arousal from hibernation in spring, these cone changes reverse. This type of natural cone remodeling may be informative as to the origin of signals within AOSLO imagery. Here, we used three different AOSLO modalities (confocal, split-detection, and dark-field) to longitudinally evaluate 13-LGS cone structure throughout the hibernation cycle and provide intra-animal comparisons of AOSLO and TEM at distinct physiological states.

2. Materials and methods

2.1. Animal Subjects and Hibernation Monitoring

The experimental procedures described were approved by the Institutional Animal Care and Use Committee of the Medical College of Wisconsin (AUA00005654) and were in accordance with the ARVO Statement for the Use of Animals in Ophthalmic and Vision Research.

Eight female and seven male 13-LGS were obtained from the University of Wisconsin Oshkosh Squirrel Colony for use in this study at the Medical College of Wisconsin. Animals were used from September to July during the 2016–2017 hibernation season, and from November to February during the 2017–2018 hibernation season. Animals used during the fall transition were kept in room temperature between the months of September and November and examined during a torpid state (called “fall transition” hereafter, Figure 1). Animals used during winter torpor (called “torpor” hereafter) were placed in a dark 4°C hibernaculum (True Manufacturing, O’Fallon, MO, USA) without food or water, and

allowed to hibernate for over 2 months before they were used for the study. Animals in the hibernaculum were checked daily for activity remotely by infrared camera (Axis Communications, Lund, Sweden), in a strategy inspired by the traditional “sawdust method” (Pengelley and Fisher, 1961) that uses the movement of sawdust placed on the back of the ground squirrel to detect activity. With our method, an image was captured of 13-LGS nests every day by the Axis Companion software (Axis Communications, Lund, Sweden). Bedding that moved from the previous day was recorded as a period of IBE. All animals used for IBE assessments were inactive (and presumably in continual torpor) for greater than 1 week. Additional daily checks were performed briefly (~2 mins) by animal care staff to check for cage condensation (indicating euthermic activity). Squirrels were removed from the hibernaculum if euthermic activity persisted for >48 hr.

Animals in fall transition or summer euthermia were kept on a natural photoperiod with light adjusted every 2 weeks to replicate day lengths in southern Wisconsin, while animals in winter torpor and IBE were kept in the constantly dark 4°C hibernaculum. Care was taken during the transport of torpid fall transition and winter animals (from the animal room or hibernaculum, respectively) to the procedural suite or room temperature housing, to limit disturbance and avoid any increase in arousal speed that is known to occur with physical stimulation (Christian et al., 2014). To verify physiological state, squirrel body temperature was measured by a FLIR E60 thermal imaging camera (FLIR Systems, Inc., Wilsonville, OR, USA) and/or by subcutaneous IPTT-300 temperature transponders (Bio Medic Data Systems, Seaford, DE, USA). To assess retinas during post-hibernation time points (1.5 hours, 24 hours, 72 hours, or 1 week), squirrels were removed from the hibernaculum and placed in room temperature in a well-lit room where they aroused to euthermia. All imaging and euthanasia were performed between the hours of 10 AM and 6 PM.

2.2. Adaptive Optics Scanning Light Ophthalmoscopy (AOSLO)

Five 13-LGS were imaged longitudinally throughout the hibernation cycle with three simultaneous AOSLO modalities (confocal, non-confocal split detection, and non-confocal dark-field). Ten 13-LGS were imaged with AOSLO at a single time-point, then subsequently used for histology. Prior to imaging, squirrels in fall transition, IBE, euthermic, and post-hibernating physiological states were anesthetized with inhaled isoflurane (up to 5% for induction in a chamber, 0.5–4% maintenance via mask delivery) in 1 L/min oxygen flow. Torpid squirrels were prepared for imaging as previously described (Sajdak et al., 2018), not requiring induction and using a 2% maintenance dose of inhaled isoflurane.

The imaged eye was first dilated and cyclopleged with phenylephrine hydrochloride (2.5%) and tropicamide (1%), and the lids were held open with a pediatric ocular speculum. Wetting drops (Saline and/or Systane (Alcon, Fort Worth, TX, USA)) were applied every 1 to 2 minutes throughout the AOSLO examinations. Images of the cone mosaic[1] were acquired using a custom AOSLO (Dubra and Sulai, 2011) modified for a 4.5 mm pupil diameter (approximate size of the dilated 13-LGS pupil). Confocal and non-confocal AOSLO videos

[1]Rod and cone photoreceptors are similar in size in the 13-LGS (von Schantz et al., 1994), and therefore difficult to distinguish with AOSLO. The superior retinal regions imaged in this study are reported to have less than 10% rod photoreceptors (Kryger et al., 1998), so we will refer to the AOSLO images as images of the cone mosaic.

of the superior retina were captured as previously described in this species (Sajdak et al., 2016). The split-detection AOSLO signal is generated from the subtraction of the two non-confocal detector intensities divided by their sum at every pixel, while the dark-field AOSLO signal is generated by averaging the two non-confocal detector intensities at every pixel (Scoles et al., 2013).

Image sequences were first collected at the horizontal optic nerve head, which has a unique pattern of pores that serve as a "roadmap" for repeated imaging of the same retinal location. Sinusoidal distortion inherent in our scanning system was estimated by imaging a Ronchi grating of known spacing, then corrected by resampling the video frames over a grid of equally-spaced pixels. The scale of the AOSLO images was determined by calculating the degrees per pixel in the resampled image of the Ronchi grating. Reference frames were automatically selected (Salmon et al., 2017), then image sequences were automatically registered and averaged to improve signal-to-noise ratio (Dubra and Harvey, 2010). The resulting images were automatically montaged with custom software employing a semi-automated SIFT-feature matching algorithm (Chen et al., 2016).

To examine changes in the cone mosaic throughout hibernation, AOSLO montages from each time point were scaled and manually aligned using Photoshop CS6 (Adobe, San Jose, CA, USA) to the largest montage using optic nerve pores and vessels, then cropped to the overlapping region and aligned again to a common 0.5 × 0.5 degree region of photoreceptors. Individual cells were semi-automatically identified from the split-detector images using the "adaptive filtering and local detection" algorithm (Cunefare et al., 2016). Cone density and Voronoi pattern were then analyzed using custom software (Mosaic Analytics, (Cooper et al., 2016a)).

2.3. Transmission Electron Microscopy (TEM)

Ten 13-LGS imaged with AOSLO at single time-points in the hibernation cycle were euthanized immediately after imaging (within 2 minutes of final image capture) by decapitation under isoflurane anesthesia. Both eyes were enucleated and the whole globe was immersion-fixed overnight in 2% paraformaldehyde plus 2% glutaraldehyde in 0.1 M sodium cacodylate buffer. Following fixation, the eyes were rinsed 3 × 5 minutes in 0.1 M cacodylate buffer.

The eyes used for TEM then had the cornea and lens removed, and sample regions were dissected from the superior retina (the location imaged with AOSLO) of the eyecup. The samples were post-fixed in 1% osmium tetroxide followed by dehydration in a graded methanol series. Subsequently, the samples were infused with acetonitrile before infiltration with Embed 812 (Electron Microscopy Sciences, Hatfield, PA, USA) and cured overnight in a 60°C oven. Then 0.5 μm sections were cut on an Ultracut E microtome (Reichert-Jung/Leica Microsystems, Wetzlar, Germany) and stained with 1% toluidine blue to ensure the sample was block-faced in the correct orientation. Both vertical cross-sections and horizontal *en face* sections were prepared from each eye imaged with AOSLO (and several contralateral eyes to serve as fixation controls). For TEM, 70 nm sections were cut using a PowerTome PT-XL ultramicrotome (RMC Boeckeler, Tucson, AS, USA), and stained with uranyl acetate and lead citrate. Imaging was performed on an H-600 transmission electron

microscope (Hitachi High Technologies, Schaumburg, IL, USA). Five cone inner segment ellipsoids and their mitochondria were manually segmented from *en face* TEM images from each animal ($n = 10$) using the Track2EM FIJI plugin (Cardona et al., 2012).

2.4. Serial Block-face Scanning Electron Microscopy (SEM) reconstruction

Two additional 13-LGS (one euthermic and one torpid) were used for scanning electron microscopy (SEM) without prior AOSLO. Fixed retina samples from the visual streak of each 13-LGS were sent in 0.1 M cacodylate buffer to Renovo Neural Inc. (Cleveland, OH, USA) for serial block-face imaging SEM. There, retinas were washed, then stained with 1% tannic acid for 30 minutes and then incubated successively with osmium ferrocyanide, thiocarbohydrazide, osmium tetroxide, and lead aspartate, as previously described (Deerinck et al., 2010; Mukherjee et al., 2016). Tissues were dehydrated and embedded in Epon resin (Electron Microscopy Sciences, Hatfield, PA, USA). Trimmed samples were imaged using a ThermoFisher Volume Scope in-chamber ultramicrotome system (ThermoFisher Scientific, Hillsboro, OR, USA) on a Teneo SEM platform using the T1 detector. On both systems, stacks of digital images were acquired at 7.0 nm/pixel resolution at 2.2 kV, using 65 nm steps; these are standard setting that produce images comparable to those from TEM systems. Each resulting serial image stack contained ~500 images (~33 μm deep, 49 × 49 μm wide). For analysis, images were scaled, and sub-stacks generated and aligned using ImageJ software with the FIJI plugin suite (Schindelin et al., 2012). Outer segment discs and mitochondria were manually segmented in 3 euthermic and 3 torpid 13-LGS cones using the Track2EM plugin (Cardona et al., 2012).

2.5. Statistical analysis

All statistical tests were performed using Prism version 7.04 (GraphPad, La Jolla, CA, USA). D-Agostino & Pearson tests were performed to test the normality of each data set and determine each statistical method. For longitudinal assessment of cone density in the same animal across 5 different physiological states, a one-way ANOVA with repeated measures was performed. For comparing cone density in two physiological states, before and after torpor, using 5 animals, a Tukey's multiple comparisons test was performed. For comparing mitochondria area fraction in TEM images, 5 cones measured from 2 animals were grouped for 5 distinct physiological states, and a one-way between groups ANOVA was performed. Measurements of outer segment volume, mitochondrial volume, and mitochondrial number from SEM image volumes were collected from 3 cones for 2 physiological states, and each did not pass the normality test, so Mann-Whitney or Kolmogorov-Smirnov tests were performed. Significance values are $^{**}P < 0.01$; $^{***}P < 0.001$; $^{****}P < 0.0001$ where relevant.

3. Results

3.1. Longitudinal Assessment of Cone Structure Throughout Hibernation

To determine how the cone mosaic changes throughout the different physiological states of hibernation, we used AOSLO to image the same retinal region in five squirrels in the five distinct physiological states. The cone mosaic was unaffected by the hibernation cycle; cone density did not significantly change in longitudinal assessments of the same region ($P =$

0.51, $n = 5$, one-way ANOVA with repeated measures, Figure 2). Two of the squirrels imaged during torpor had poor image quality, which affected cell identification (Figure 2). Figure 3 shows a representative location of 13-LGS retina longitudinally assessed with AOSLO. Average cone density was not significantly different when comparing before (fall transition) and after (24 hrs post-hibernation) torpor (mean ± SD difference = 5.3 ± 3.5 cells/deg^2, $P = 0.58$, $n = 5$, Tukey's multiple comparisons test), and cell packing was consistent between states as well (Figure 3).

A very small subset of individual photoreceptors (4 out of ~17,500 visible before and after hibernation) became progressively undetectable with any of the AOSLO modalities after hibernation. Figure 3 shows an example of a photoreceptor (presumed cone) that became progressively undetectable by AOSLO after arousal from hibernation. Interestingly, the reflective properties of the photoreceptor were visible with confocal AOSLO at 24 hours post- hibernation, and this reflectance was lost 72 hours post-hibernation. Residual structure was visible by split-detection and dark-field AOSLO at 72 hours post-hibernation. At the euthermic assessment 4 months after hibernation, the residual structure became undetectable in all three AOSLO modalities.

3.2. Intra-animal in vivo and ex vivo Assessment of Photoreceptors Throughout Hibernation

Figure 4 shows intra-animal comparisons of the cone mosaic with confocal AOSLO and outer segment structure with TEM. The level of confocal AOSLO signal disruption and outer segment organization were often associated. Confocal AOSLO signal was most disrupted during torpor and 1.5 hours after hibernation, and TEM of cones revealed reduced and disorganized outer segment disc structure during these physiological states (Figure 4). However, cone outer segment disc disruption was also observed during fall transition, without severe disruption in confocal AOSLO (Figure 4). Further, confocal AOSLO signal and cone structure seem to recover during the brief periods of IBE (Figure 4), suggesting that outer segment discs recover during these ~12–24 hour periods of increased metabolic activity. By 1 week after hibernation, confocal AOSLO signal appeared normal and cone outer segment discs recovered and extended to the distal tips of the cone sheath.

We investigated the relationship between split-detection AOSLO signal and mitochondrial volume using the same regions examined in Figure 4. Cones were detectable using split-detection AOSLO throughout the seasonal cycle (Figure 5A), despite the variability in confocal AOSLO signal at the same locations (Figure 4A). Cone mitochondria visualized by TEM were sparser in pre-hibernation, torpor, and 1.5 hours after hibernation, but appeared more abundant during IBE and 1 week post-hibernation (Figure 5B). To examine this quantitively, mitochondria were segmented within the inner segment ellipsoid at each physiological state (Figures 5C-D), revealing significantly increased mitochondrial area fraction (mitochondria area ÷ inner segment ellipsoid area)during IBE relative to all other physiological states (Figure 5D). While the mitochondrial volume was reduced in fall transition and torpor, and did not recover by 1.5 hours after hibernation, cone mitochondria were larger in those two metabolically-suppressed states compared to mitochondria in IBE and 1 week after hibernation (Figure 5B).

3.3. Cone Outer Segment and Inner Segment 3D Comparisons in Euthermic and Torpid Retina

We examined outer segment disc and inner segment mitochondrial volumes in cones from one euthermic and one torpid 13-LGS retina using 3D SEM segmentations. Figures 6A-B show the 3D SEM segmentations of outer segment discs and inner segment mitochondria bundles used for this analysis. Outer segment disc volume was 30.84 ± 2.72 μm^3 and 24.85 ± 4.25 μm^3 in cones from euthermic and torpid 13-LGS, respectively, supporting outer segment disc reduction seen in other studies, although the outer segment disc reduction was not significant ($P = 0.2$, $n = 3$ cone outer segments each, Mann Whitney test). No completely absent outer segments were seen in any torpid SEM (or TEM) samples in this study, suggesting that while outer segments are indeed variably disrupted, outer segment discs are not commonly eliminated completely within the cone outer segment sheath. Mitochondrial volume was 0.43 ± 0.32 μm^3 (3 cones, $n = 337$ mitochondria) and 0.54 ± 0.35 μm^3 (3 cones, $n = 402$ mitochondria) in cones from euthermic and torpid 13-LGS, respectively; a significant increase in the volume of torpid mitochondria ($P = < 0.0001$, Mann-Whitney test; Figure 6). The number of mitochondria in these cells was highly variable and not significantly different between the euthermic and torpid samples ($P = 0.60$, Kolmogorov-Smirnov test; Figures 6A-C).

Discussion

The multiple physiological states of the 13-LGS hibernation cycle provide a natural model to investigate cellular adaptations to drastic metabolic fluctuations. Here, we report the non-invasive assessment of cone photoreceptor structural changes with cellular resolution AOSLO imaging during several distinct states of the seasonal cycle. We also provide intra-animal comparisons of cone structure with AOSLO imaging and TEM. To the best of our knowledge, this is this first attempt to examine structural changes of cones during hibernation with *in vivo* AOSLO imaging, and the first assessments of cone structure during intermediary states of the 13-LGS seasonal cycle (fall transition and IBE).

Kuwabara (1975) was the first to examine ground squirrel cones during hibernation. He observed shortening of cone outer segments without an increase in retinal pigment epithelium (RPE) phagosomes (Kuwabara, 1975). After two months of hibernation, cone outer segments were “almost absent in several animals” (Kuwabara, 1975), and cone structure fully recovered two weeks after hibernation. Two years later, Remé and Young (1977) described a more subtle shortening of cone outer segments, and also showed a reduction in the size and number of cone inner segment ellipsoid mitochondria. Mitochondrial size and number returned to euthermic levels 3 days after hibernation, while outer segment length followed suit 7 days after hibernation (Remé and Young, 1977).

Consistent with these reports, we demonstrate reversible cone degeneration during the 13-LGS annual hibernation cycle. Like Remé and Young and previous observations in our laboratory (Sajdak et al., 2018), we did not observe a complete disappearance of outer segments, but rather, highly variable disc remodeling (*e.g.* narrowed and clumped discs) within an intact cone sheath (Figure 4C, Figure 6). We find that this cone outer segment disc remodeling starts prior to the 13-LGS being introduced into a cold environment (Figure 4).

This transitional period between homeothermic and heterothermic physiology is often overlooked in hibernation studies. This period of fall transition occurs prior to cold exposure, where many 13-LGS undergo fall torpor bouts of varying length and frequency (Russell et al., 2010). We specifically selected animals that were in the fall transition torpid state (Figure 1) and found disorganized outer segment disc structure (Figure 4C), further evidence that 13-LGS cannot be considered “euthermic normal” during this period of fall transition (Russell et al., 2010)

Similar to Remé and Young (1977), our TEM analysis suggested reduced mitochondrial number in the torpid state (Figure 5). However, when examining the entire mitochondrial structure in 3D using SEM, we found that mitochondria were increased in volume during torpor compared to euthermic 13-LGS (Figure 6). An increase in mitochondrial volume in torpid 13-LGS conflicts with the current idea that “mitochondria are diminished in size” as seen with 2D TEM analysis (Remx and Young, 1977), and decreased volume in hibernating mitochondria (Kaden et al., 2013; Li et al., 2017). Our SEM data are limited to three cones each in one euthermic and one torpid 13-LGS. In addition, the SEM sectioning was done in different planes for the two samples (Figures 6A-B), which could confound the 3D registration, manual segmentation, and resulting volume measurements seen. Together, our SEM data highlight a need for this type of 3D analysis to characterize changes at the level of individual cone photoreceptor mitochondria. More work is needed to define mitochondrial morphology in a population of euthermic 13-LGS, then assess how the morphology changes in each of the physiological states throughout the hibernation cycle (Figure 1).

Using 2D TEM, the only significant increase in mitochondrial area relative to winter torpor was during IBE (Figure 5). Surprisingly, not only was mitochondrial area higher during IBE compared to all other physiological states examined (Figure 5C), but outer segment structure seemed to recover as well (Figure 4C). IBE periods last about 12 to 24 hours and occur every 1 to 2 weeks (e.g. Figure 1, (Staples, 2016)). Since we tracked daily movement of each squirrel to determine if an IBE had occurred, our temporal data are limited to every 24 hours. Therefore, while each IBE examined was of the expected rhythmicity relative to the previous IBE (1 to 2 weeks), we cannot know precisely when the IBE data were collected relative to its preceding torpor bout. Since the animals we examined during IBE had body temperatures of 35–37°C, and the IBE time-course is well-established (Staples, 2016), we conservatively estimate IBE collection time-points were within a window of 2 to 24 hours.

Given this window of time, it is somewhat surprising to find nearly complete recovery of the cone outer segment structure examined with AOSLO and TEM during states of IBE (Figure 4). Cone outer segment renewal rate in euthermic mammals has been estimated to range from 1 – 2.7 μm / day (Jonnal et al., 2010; Long et al., 1986). Rod photoreceptor disc radiolabeling suggests a similar rate of outer segment renewal (frog: 1.5 – 3.8 μm / day (Besharse et al., 1977)). A complete renewal of an ~8 μm 13-LGS cone outer segment during these IBE states would thus require renewal rates more than twice as fast as these established rates. With an increased recruitment in mitochondria (Figure 5C) and up to 88% of total ground squirrel energy throughout hibernation being used during IBEs (Staples, 2014; Wang and Wolowyk, 1988), it is conceivable that cone outer segments grow at an accelerated rate during this rapid shift in metabolic state. Alternatively, it is possible that the

altered outer segment structure in torpid states makes this region more susceptible to variable disruption during histological processing. Alternative approaches such as cryoelectron tomography may limit potentially artefactual outer segment changes (Nickell et al., 2007). Our data warrant further investigation into this process of cone regeneration during IBE and post-hibernation physiological states, ideally with continuous monitoring of physiological states to more accurately detect transition periods. For example, electrocardiogram telemetry measurements of heart rate was found to be more sensitive at detecting IBE compared to measuring body temperature (MacCannell et al., 2018). Since torpid and IBE states are experienced in complete darkness, we expect a minimal influence from a typical light-dark shedding cycle. Indeed, previous hibernation studies suggest that circadian rhythms are inhibited during hibernation (Revel et al., 2007; Williams et al., 2012), but the extent to which photoreceptor disc shedding cycles change during hibernation is not known.

Overall, the ground squirrel cone mosaic is unaffected by the hibernation cycle (Figures 2 & 3), meaning that cones do not degenerate completely, but that intact outer segment sheaths and inner segments remain in an unperturbed mosaic despite the changes to subcellular structures within (i.e. outer segment discs and inner segment mitochondria). The rare cone that becomes undetectable into the summer months (Figure 3) likely represents no consequence to a squirrel's vision, given that visual acuity in humans is not abnormal until cone density is 38–62% below normal (Ratnam et al., 2013; Sun et al., 2016). These voids seem to persist in the mosaic, as no cell migration into these spaces was observed. This suggests that either these cones are altered in a way that affects their AOSLO detection properties, or that the cone outer segments and inner segments have degenerated. The former scenario may be more likely, given that rods expand to fill vacant photoreceptor space in humans (Curcio et al., 1993; Hansen et al., 2013). However, it is not known if this kind of photoreceptor migration occurs in cone-dominated mosaics.

Photoreceptor structure visualized with split-detection AOSLO imaging is thought to arise from the photoreceptor inner segment due to its similarity to the appearance and diameter of inner segments visualized with Nomarski differential interference contrast imaging (Scoles et al., 2014). Non-reflective cones are thought to have absent or altered outer segments, which affects confocal AOSLO signal but not multiply-scattered light detected with non-confocal AOSLO (*e.g.* split-detection AOSLO) (Langlo et al., 2017; Sun et al., 2016). However, little is known about how/if mitochondria are involved in these signals. Our results indicate that any changes in inner segment mitochondria occurring during hibernation do not prevent visualization of inner segments by split-detection AOSLO (Figures 2, 3, & 5). Image quality of split-detection images was reduced during torpor and 1.5 hours post-hibernation imaging (Figures 3 & 5A), but cells were still detectable during these and all other physiological states examined. Changes to the anterior segment, like corneal stroma thickening during torpor (Sajdak et al., 2018), likely diminish AOSLO image quality during torpid states.

Cone reflectance detected with confocal AOSLO is thought to arise from the concomitant waveguiding properties of the cone (Jonnal et al., 2007; Scoles et al., 2014). We reasoned that outer segment disruption throughout hibernation would affect the waveguiding

properties of the cones and alter confocal AOSLO signal. Indeed, confocal AOSLO images of the cone mosaic were disrupted when examining 13-LGSs in fall transition torpor, winter torpor, and 1.5 hours post-hibernation (arousal to euthermia), compared to IBE, 24 hours post-hibernation, and thereafter (Figures 3 & 4). Considering the intra-animal structural changes in outer segment discs seen with TEM and AOSLO at the same retinal regions, we conclude that intact outer segments are not required to visualize inner segments with split-detection AOSLO. This was suspected based on the initial observations in patients with achromatopsia (Scoles et al., 2014) in whom histological validation was not possible. These *in vivo* to *ex vivo* comparisons have scaling limitations, in that axial length was not measured in the animals and therefore scale is approximated by degrees, or microns using an assumed axial length of 7.9 mm (axial length of the European ground squirrel (Hughes, 1977).

Recent reports suggest that such “dysflective” cones can be functional despite the absence of reflective properties detectable with confocal AOSLO (Bruce et al., 2015; Tu et al., 2017; Wang et al., 2015). Future work should assess *in vivo* cone function by measuring responses to light stimuli (Cooper et al., 2017) to examine what degree of structure is required for cone function and how rapidly cone function recovers in regenerating 13-LGS cones.

Acknowledgements:

The authors thank Tiffany Butler, Lisa King, Christine Skumatz, Joseph Thulin, and the Biomedical Resource Center at MCW for their contributions to ground squirrel care, Rob Goodwin for help preparing TEM samples, Emily Benson and Grahame Kidd for preparing and imaging the SEM samples, Rob Cooper for developing and supporting the Mosaic Analytics program, and Joseph Besharse for the helpful discussions related to EM interpretation.

Grant Information: Research in the manuscript was supported by the National Eye Institute of the National Institutes of Health (NIH) under award numbers P30EY001931, T32EY014537, U01EY025477, and U24EY029891. This investigation was conducted in a facility constructed with support from Research Facilities Improvement Program Grant Number C06RR016511 from the National Center for Research Resources, NIH. The content is solely the responsibility of the authors and does not necessarily represent the official views of the NIH. Additional support from the Foundation Fighting Blindness consortium PPA-0641–0718-UCSF, the Alcon Research Institute, and the Gene & Ruth Posner Foundation.

References

Andrews MT, 2007 Advances in molecular biology of hibernation in mammals. BioEssays 29, 431–440. 10.1002/bies.20560. [PubMed: 17450592]

Besharse JC, Hollyfield JG, Rayborn ME, 1977 Turnover of rod photoreceptor outer segments. II. Membrane addition and loss in relationship to light. Journal of Cell Biology 75, 507–527. [PubMed: 264121]

Bruce KS, Harmening WM, Langston BR, Tuten WS, Roorda A, Sincich LC, 2015 Normal perceptual sensitivity arising from weakly reflective cone photoreceptors. Investigative Ophthalmology & Visual Science 56, 4431–4438. 10.1167/iovs.15-16547. [PubMed: 26193919]

Cardona A, Saalfeld S, Schindelin J, Arganda-Carreras I, Preibisch S, Longair M, Tomancak P, Hartenstein V, Douglas RJ, 2012 TrakEM2 software for neural circuit reconstruction. PLoS One 7, e38011 10.1371/journal.pone.0038011. [PubMed: 22723842]

Carey HV, Andrews MT, Martin SL, 2003 Mammalian hibernation: cellular and molecular responses to depressed metabolism and low temperature. Physiological Reviews 83, 1153–1181. [PubMed: 14506303]

Carroll J, Choi SS, Williams DR, 2008 In vivo imaging of the photoreceptor mosaic of a rod monochromat. Vision Research 48, 2564–2568. 10.1016/j.visres.2008.04.006. [PubMed: 18499214]

Chen M, Cooper RF, Han GK, Gee J, Brainard DH, Morgan JI, 2016 Multi-modal automatic montaging of adaptive optics retinal images. Biomedical Optics Express 7, 4899–4918. 10.1364/BOE.7.004899. [PubMed: 28018714]

Christian SL, Rasley BT, Roe T, Moore JT, Harris MB, Drew KL, 2014 Habituation of Arctic ground squirrels (Urocitellus parryii) to handling and movement during torpor to prevent artificial arousal. Frontiers in Physiology 9, Article 174. 10.3389/fphys.2014.00174.

Cooper RF, Tuten WS, Dubra A, Brainard DH, Morgan JIW, 2017 Non-invasive assessment of human cone photoreceptor function. Biomedical Optics Express 8, 5098–2112. 10.1364/BOE.8.005098. [PubMed: 29188106]

Cooper RF, Wilk MA, Tarima S, Carroll J, 2016 Evaluating descriptive metrics of the human cone mosaic. Investigative Ophthalmology & Visual Science 57, 2992–3001. 10.1167/iovs.16-19072. [PubMed: 27273598]

Cunefare D, Cooper RF, Higgins B, Katz DF, Dubra A, Carroll J, Farsiu S, 2016 Automatic detection of cone photoreceptors in split detector adaptive optics scanning light ophthalmoscope images. Biomedical Optics Express 7, 2036–2050. 10.1364/BOE.7.002036. [PubMed: 27231641]

Curcio CA, Millican CL, Allen KA, Kalina RE, 1993 Aging of the human photoreceptor mosaic: evidence for selective vulnerability of rods in central retina. Investigative Ophthalmology & Visual Science 34, 3278–3296. [PubMed: 8225863]

Deerinck TJ, Bushong EA, Lev-Ram V, Shu X, Tsien RY, Ellisman MH, 2010 Enhancing serial block-face scanning electron microscopy to enable high resolution 3-D nanohistology of cells and tissues. Microscopy and Microanalysis 16, 1138–1139.

Dubra A, Harvey Z, 2010 Registration of 2D images from fast scanning ophthalmic instruments, in: Fischer B, Dawant B, Lorenz C (Eds.), Biomedical Image Registration, 1 ed. Springer-Verlag, Berlin, pp. 60–71.

Dubra A, Sulai Y, 2011 Reflective afocal broadband adaptive optics scanning ophthalmoscope. Biomedical Optics Express 2, 1757–1768. [PubMed: 21698035]

Hansen SO, Cooper RF, Dubra A, Carroll J, Weinberg DV, 2013 Selective cone photoreceptor injury in acute macular neuroretinopathy. Retina 33, 1650–1658. 10.1097/IAE.0b013e31828cd03a. [PubMed: 23615345]

Horton JC, Parker AB, Botelho JV, Duncan JL, 2015 Spontaneous regeneration of human photoreceptor outer segments. Scientific Reports 5 10.1038/srep12364.

Hughes A, 1977 The topography of vision in animals with contrasting life styles, in: Crescitelli F (Ed.), Handbook of Sensory Physiology. Springer, Berlin, pp. 614–642.

Jagger WS, 1985 Visibility of photoreceptors in the intact living cane toad eye. Vision Research 25, 729–731. [PubMed: 3927588]

Jonnal RS, Besecker JR, Derby JC, Kocaoglu OP, Cense B, Gao W, Wang Q, Miller DT, 2010 Imaging outer segment renewal in living human cone photoreceptors. Optics Express 18, 5257–5270. 10.1364/OE.18.005257. [PubMed: 20389538]

Jonnal RS, Rha J, Zhang Y, Cense B, Gao W, Miller DT, 2007 In vivo functional imaging of human cone photoreceptors. Optics Express 14, 16141–16160.

Kaden T, Du J, Goel A, Lu G, Li W, 2013 Structural and functional properties of photoreceptor mitochondria in awake and hibernating ground squirrels. Investigative Ophthalmology & Visual Science 54, E-abstract: 6082.

Kryger Z, Galli-Resta L, Jacobs GH, Reese BE, 1998 The topography of rod and cone photoreceptors in the retina of the ground squirrel. Visual Neuroscience 15, 685–691. [PubMed: 9682870]

Kuwabara T, 1975 Cytologic changes of the retina and pigment epithelium during hibernation. Investigative Ophthalmology 14, 457–467. [PubMed: 166050]

Land MF, Snyder AW, 1985 Cone mosaic observed directly through natural pupil of live vertebrate. Vision Research 25, 1519–1523. [PubMed: 4090286]

Langlo CS, Erker LR, Parker M, Patterson EJ, Higgins BP, Summerfelt P, Razeen MM, Collison FT, Fishman GA, Kay CN, Zhang J, Weleber RG, Yang P, Pennesi ME, Lam BL, Chulay JD, Dubra A, Hauswirth WW, Wilson DJ, Carroll J, ACHM-001 Study Group, 2017 Repeatability and longitudinal assessment of foveal cone structure in CNGB3-associated achromatopsia. Retina, 1956–1966. 10.1097/IAE.0000000000001434.

Li W, Ball J, Chen S, 2017 Cone mitochondria enhance light transmission. Investigative Ophthalmology & Visual Science 58, E-Abstract: 1037. [PubMed: 28192795]

Long KO, Fisher SK, Fariss RN, Anderson DH, 1986 Disc shedding and autophagy in the cone-dominant ground squirrel retina. Experimental Eye Research 43, 193–205. [PubMed: 3758219]

MacCannell ADV, Jackson EC, Mathers KE, Staples JF, 2018 An improved method for detecting torpor entrance and arousal in a mammalian hibernator using heart rate data. Journal of Experimental Biology 221, jeb174508 10.1242/jeb.174508. [PubMed: 29361606]

Merriman DK, Lahvis G, Jooss M, Gesicki JA, Schill K, 2012 Current practices in a captive breeding colony of 13-lined ground squirrels (Ictidomys tridecemlineatus). 41, 315–325. 10.1038/laban.150.

Merriman DK, Sajdak BS, Li W, Jones BW, 2016 Seasonal Lab animal and post-trauma remodeling in cone-dominant ground squirrel retina. Experimental Eye Research 150, 90–105. 10.1016/j.exer.2016.01.011. [PubMed: 26808487]

Miller DT, Williams DR, Morris GM, Liang J, 1996 Images of cone photoreceptors in the living human eye. Vision Research 36, 1067–1079. [PubMed: 8762712]

Mukherjee R, Clark HR, Chavan V, Benson EK, Kidd GJ, Srivastava S, 2016 Analysis of brain mitochondria using serial block-face scanning electron microscopy. Journal of Visualized Experiments. 10.3791/54214.

Nickell S, Park PS, Baumeister W, Palczewski K, 2007 Three-dimensional architecture of murine rod outer segments determined by cryoelectron tomography. Journal of Cell Biology 177, 917–925. 10.1083/jcb.200612010. [PubMed: 17535966]

Pallikaris A, Williams DR, Hofer H, 2003 The reflectance of single cones in the living human eye. Investigative Ophthalmology & Visual Science 44, 4580–4592. [PubMed: 14507907]

Pengelley ET, Fisher KC, 1961 Rhythmical arousal from hibernation in the gold-mantled ground squirrel, *Citellus lateralis tescorum*. Canadian Journal of Zoology 39, 105–120.

Ratnam K, Carroll J, Porco TC, Duncan JL, Roorda A, 2013 Relationship between foveal cone structure and clinical measures of visual function in patients with inherited retinal degenerations. Investigative Ophthalmology & Visual Science 54, 5836–5847. 10.1167/iovs.13-12557. [PubMed: 23908179]

Remé CE, Young RW, 1977 The effects of hibernation on cone visual cells in the ground squirrel. Investigative Ophthalmology & Visual Science 16, 815–840. [PubMed: 893032]

Revel FG, Herwig A, Garidou ML, Dardente H, Menet JS, Masson-Pevet M, Simonneaux V, Saboureau M, Pevet P, 2007 The circadian clock stops ticking during deep hibernation in the European hamster. Proceedings of the National Academy of Sciences of the United States of America 104, 13816–13820. [PubMed: 17715068]

Roorda A, Duncan JL, 2015 Adaptive optics ophthalmoscopy. Annual Review of Vision Science 1, 19–50. 10.1146/annurev-vision-082114-035357.

Roorda A, Romero-Borja F, Donnelly WJ 3rd, Queener H, Hebert T, Campbell M, 2002 Adaptive optics scanning laser ophthalmoscopy. Optics Express 10, 405–412. [PubMed: 19436374]

Russell RL, H. P, O. N, Epperson LE, Martin SL, 2010 Extensive use of torpor in 13-lined ground squirrels in the fall prior to cold exposure. Journal of Comparative Physiology B 180, 1165–1172. 10.1007/s00360-010-0484-8.

Sajdak B, Sulai YN, Langlo CS, Luna G, Fisher SK, Merriman DK, Dubra A, 2016 Noninvasive imaging of the thirteen-lined ground squirrel photoreceptor mosaic. Visual Neuroscience 33, e003 10.1017/S0952523815000346. [PubMed: 26923645]

Sajdak BS, Bell BA, Lewis TR, Luna G, Cornwell GS, Fisher SK, Merriman DK, Carroll J, 2018 Assessment of outer retinal remodeling in the hibernating 13-lined ground squirrel. Investigative Ophthalmology & Visual Science 59, 2538–2547. [PubMed: 29847661]

Salmon AE, Cooper RF, Langlo CS, Baghaie A, Dubra A, Carroll J, 2017 An automated reference frame selection (ARFS) algorithm for cone imaging with adaptive optics scanning light ophthalmoscopy. Translational Vision Science & Technology 6, 9 10.1167/tvst.6.2.9.

Schindelin J, Arganda-Carreras I, Frise E, Kaynig V, Longair M, Pietzsch T, Preibisch S, Rueden C, Saalfeld S, Schmid B, Tinevez JY, White DJ, Hartenstein V, Eliceiri K, Tomancak P, Cardona A, 2012 Fiji: An open-source platform for biological-image analysis. Nature Methods 9, 676–682. 10.1038/nmeth.2019. [PubMed: 22743772]

Scoles D, Sulai YN, Dubra A, 2013 In vivo dark-field imaging of the retinal pigment epithelium cell mosaic. Biomedical Optics Express 4, 1710–1723. 10.1364/BOE.4.001710. [PubMed: 24049692]

Scoles D, Sulai YN, Langlo CS, Fishman GA, Curcio CA, Carroll J, Dubra A, 2014 In vivo imaging of human cone photoreceptor inner segments. Investigative Ophthalmology & Visual Science 55, 4244–4251. 10.1167/iovs.14-14542. [PubMed: 24906859]

Song H, Rossi EA, Latchney L, Bessette A, Stone E, Hunter JJ, Williams DR, Chung M, 2015. Cone and rod loss in Stargardt disease revealed by adaptive optics scanning light ophthalmoscopy. JAMA Ophthalmology 133, 1198–1203. 10.1001/jamaophthalmol.2015.2443. [PubMed: 26247787]

Staples JF, 2014 Metabolic suppression in mammalian hibernation: the role of mitochondria. Journal of Experimental Biology 217, 2032–2036. 10.1242/jeb.092973. [PubMed: 24920833]

Staples JF, 2016 Metabolic flexibility: hibernation, torpor, and estivation. Comprehensive Physiology 6, 737–771. 10.1002/cphy.c140064. [PubMed: 27065167]

Sun LW, Johnson RD, Langlo CS, Cooper RF, Razeen MM, Russillo MC, Dubra A, Connor TB Jr., Han D, Pennesi ME, Kay CN, Weinberg DV, Stepien KE, Carroll J, 2016 Assessing photoreceptor structure in retinitis pigmentosa and Usher syndrome. Investigative Ophthalmology & Visual Science 57, 2428–2442. 10.1167/iovs.15-18246. [PubMed: 27145477]

Tu JH, Foote KG, Lujan BJ, Ratnam K, Qin J, Gorin MB, Cunningham ET Jr., Tuten WS, Duncan JL, Roorda A, 2017 Dysflective cones: Visual function and cone reflectivity in long-term follow-up of acute bilateral foveolitis. American Journal of Ophthalmology Case Reports 7, 14–19. 10.1016/j.ajoc.2017.04.001. [PubMed: 29057371]

von Schantz M, Szél A, van Veen T, Farber DB, 1994 Expression of phototransduction cascade genes in the ground squirrel retina. Investigative Ophthalmology & Visual Science 35, 2558–2566. [PubMed: 7512947]

Wade AR, Fitzke FW, 1998 In vivo imaging of the human cone-photoreceptor mosaic using a confocal laser scanning ophthalmoscope. Lasers and Light in Ophthalmology 8, 129–136.

Wang LCH, Wolowyk MW, 1988 Torpor in mammals and birds. Canadian Journal of Zoology 66, 133–137.

Wang Q, Tuten WS, Lujan BJ, Holland J, Bernstein PS, Schwartz SD, Duncan JL, Roorda A, 2015 Adaptive optics microperimetry and OCT images show preserved function and recovery of cone visibility in macular telangiectasia type 2 retinal lesions. Investigative Ophthalmology & Visual Science 56, 778–786. 10.1167/iovs.14-15576. [PubMed: 25587056]

Williams CT, Barnes BM, Richter M, Buck CL, 2012 Hibernation and circadian rhythms of body temperature in free-living Arctic ground squirrels. Physiological and Biochemical Zoology 85, 397–404. [PubMed: 22705489]

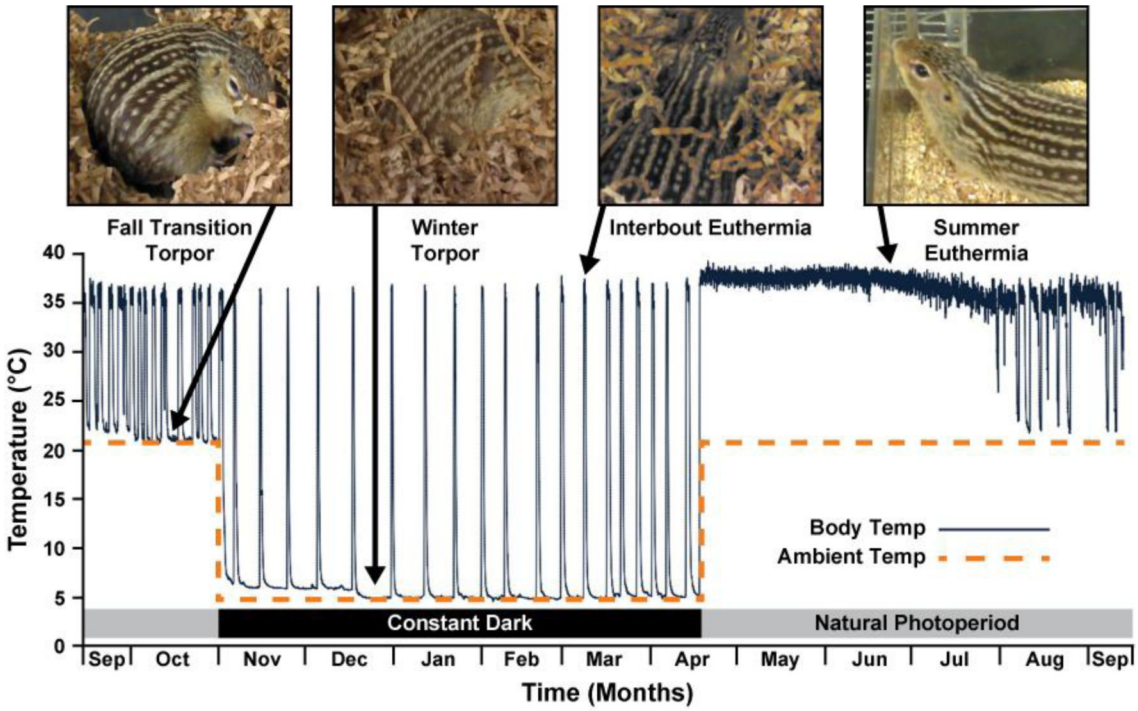

Figure 1 –.

Illustration of physiological states of the 13-lined ground squirrel seasonal cycle. Body temperature (solid line) of 1 animal measured in two ambient temperature environments (dashed line; 5°C starting November, and 21°C starting in April). Fall transition varies in onset and frequency between animals (Russell et al., 2010), but often includes periodic reductions in body temperature and metabolic activity while in room temperature (21°C). Periods of interbout euthermia occur every ~1–2 weeks. This figure was adapted with permission from (Cooper et al., 2016b; Vermillion et al., 2015). Copyright (2015) American Chemical Society. Body temperature was not continuously measured in our study.

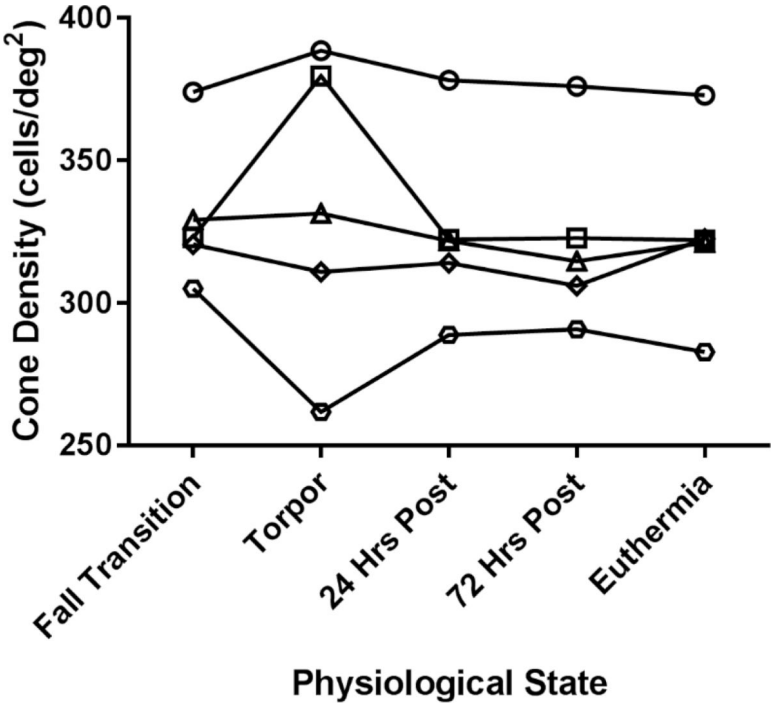

Figure 2 –.

Longitudinal assessment of cone density, just superior to the optic nerve head, in 5 different animals. Only two cone density measurements (from images captured in torpid animals) appeared to deviate, although cone density did not change significantly ($P = 0.51$, $n = 5$, one-way ANOVA with repeated measures). Density was calculated in degrees, but the y axis can be estimated to range from 25,000 to 40,000 cells/mm^2 when assuming a retinal magnification factor of 100 μm/degree (based on the 7.90 mm axial length of the European ground squirrel (Hughes, 1977)).

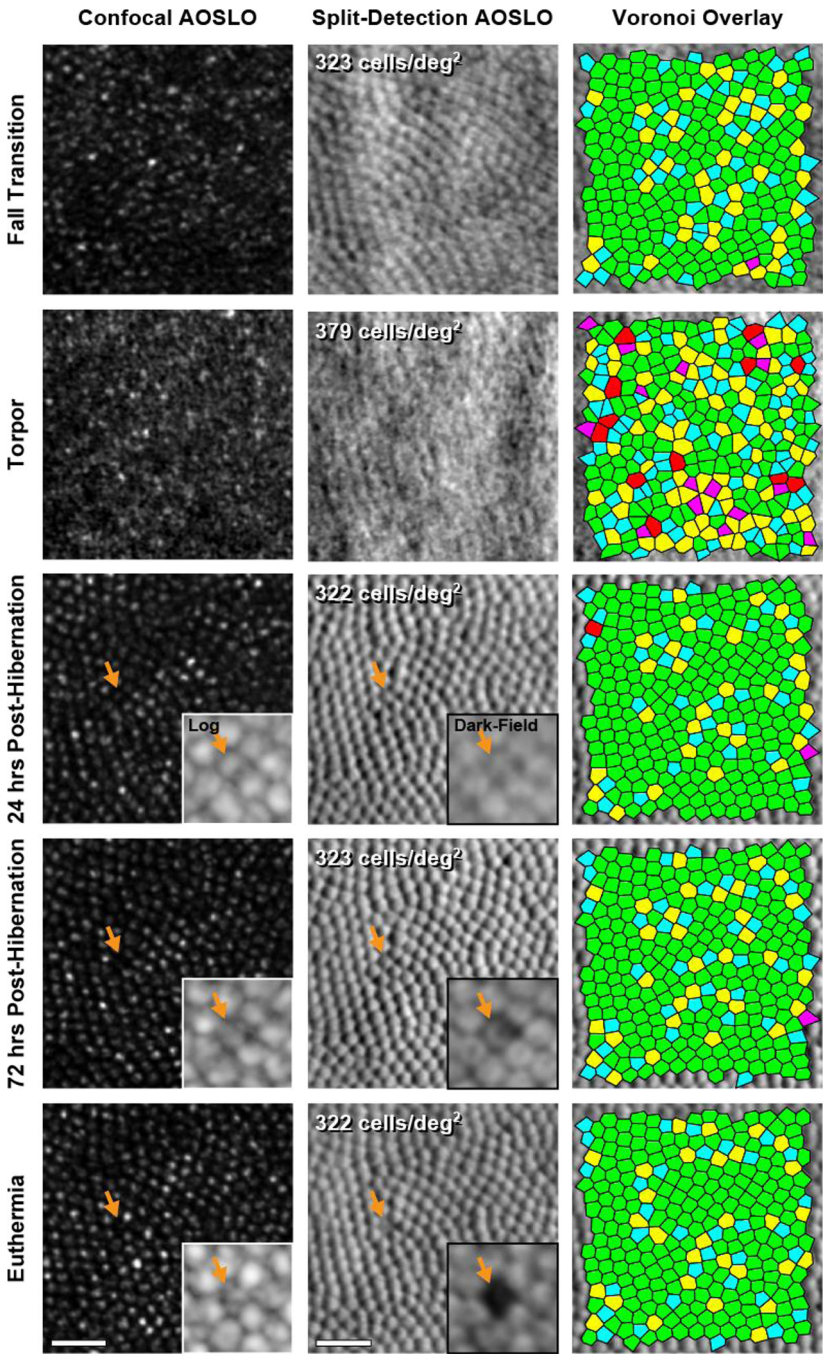

Figure 3 –.

Longitudinal assessment of the photoreceptor mosaic throughout the 13-LGS seasonal cycle. Photoreceptor reflectivity in confocal AOSLO (left column) is disrupted during a metabolically suppressed state of fall transition, and this disruption increases during torpor. Despite these changes, cone density measured from split-detection AOSLO images (center column) did not change before and after torpor. Rarely, a non-waveguiding photoreceptor will become undetectable by split-detection AOSLO, leaving a gap rather than maintaining residual structure (orange arrows). Insets show close-up images of the cone with

progressively extinguished AOSLO signal (confocal inset in log scale; split-detection inset is dark-field). 72 hours after hibernation this cone is not reflective, but has residual structure seen with non-confocal AOSLO (split-detection and dark-field). Interestingly, this cone has altered dark-field signal at 72 hours, then progresses to undetectable in the euthermic state (4 months after hibernation), creating a gap in the mosaic easily seen with dark-field AOSLO. Voronoi overlays (right column) show that cell packing remained constant before and after torpor (44.1% six-sided cells in torpor, compared to 73.5 ± 3.8% (mean ± SD) six-sided cells in all other physiological states in this animal). Number of sides in Voronoi overlay: pink = 4-sides, blue = 5-sides, green = 6-sides, yellow = 7 sides, red = 8 sides. It is difficult to distinguish structural changes from reduced image quality in the torpid time-point in this example, but structure appeared “euthermic-like” just 24 hours after torpor. Scale bars = 20 μm.

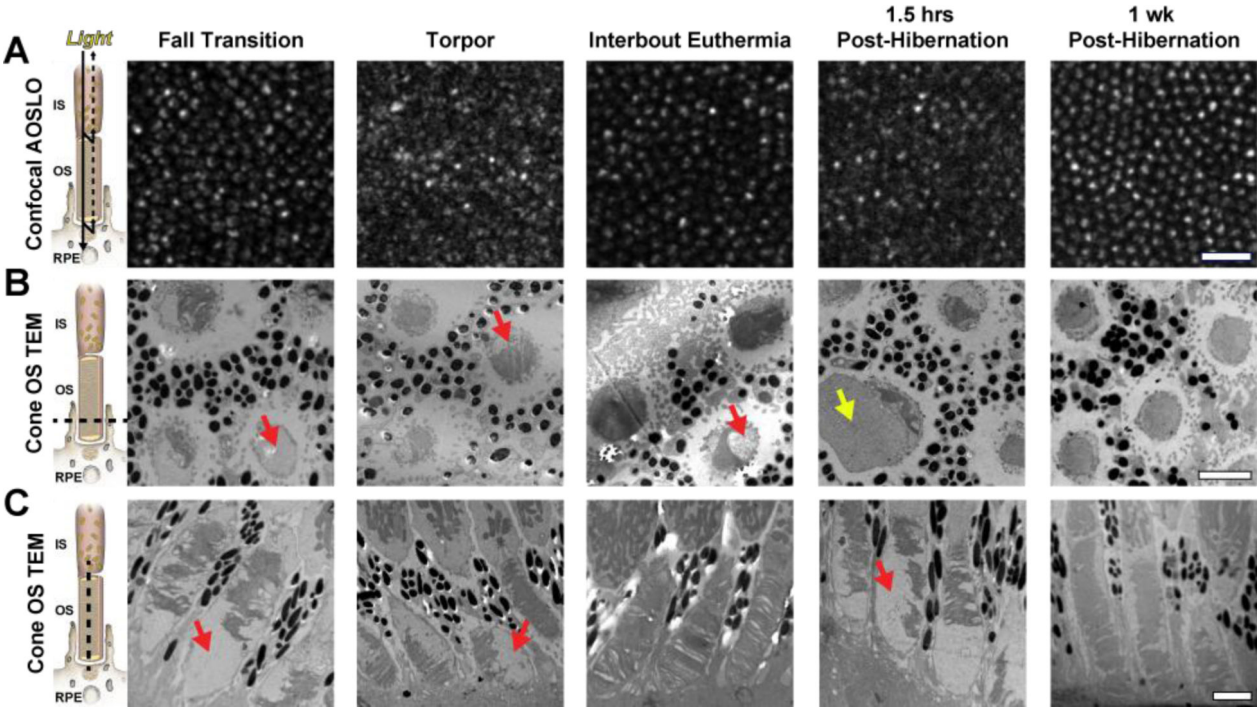

Figure 4 –.

Intra-animal comparisons of confocal AOSLO (A), transverse/horizontal TEM outer segment (OS) sections (B), and longitudinal/vertical TEM OS sections (C) in different physiological states. Photoreceptor schematic in (A) is based off of a model presented by (Jonnal et al., 2007), in which the confocal signal is thought to arise from the waveguiding properties of the photoreceptor; whereas the schematics in (B) and (C) show the photoreceptor plane visualized with TEM (dashed line). Disruptions in OS structure (red arrows) and abnormally enlarged structures (yellow arrow) may disrupt the normal waveguide properties of photoreceptors and affect their confocal AOSLO signal. AOSLO scale bar = 20 μm. TEM scale bars = 2 μm.

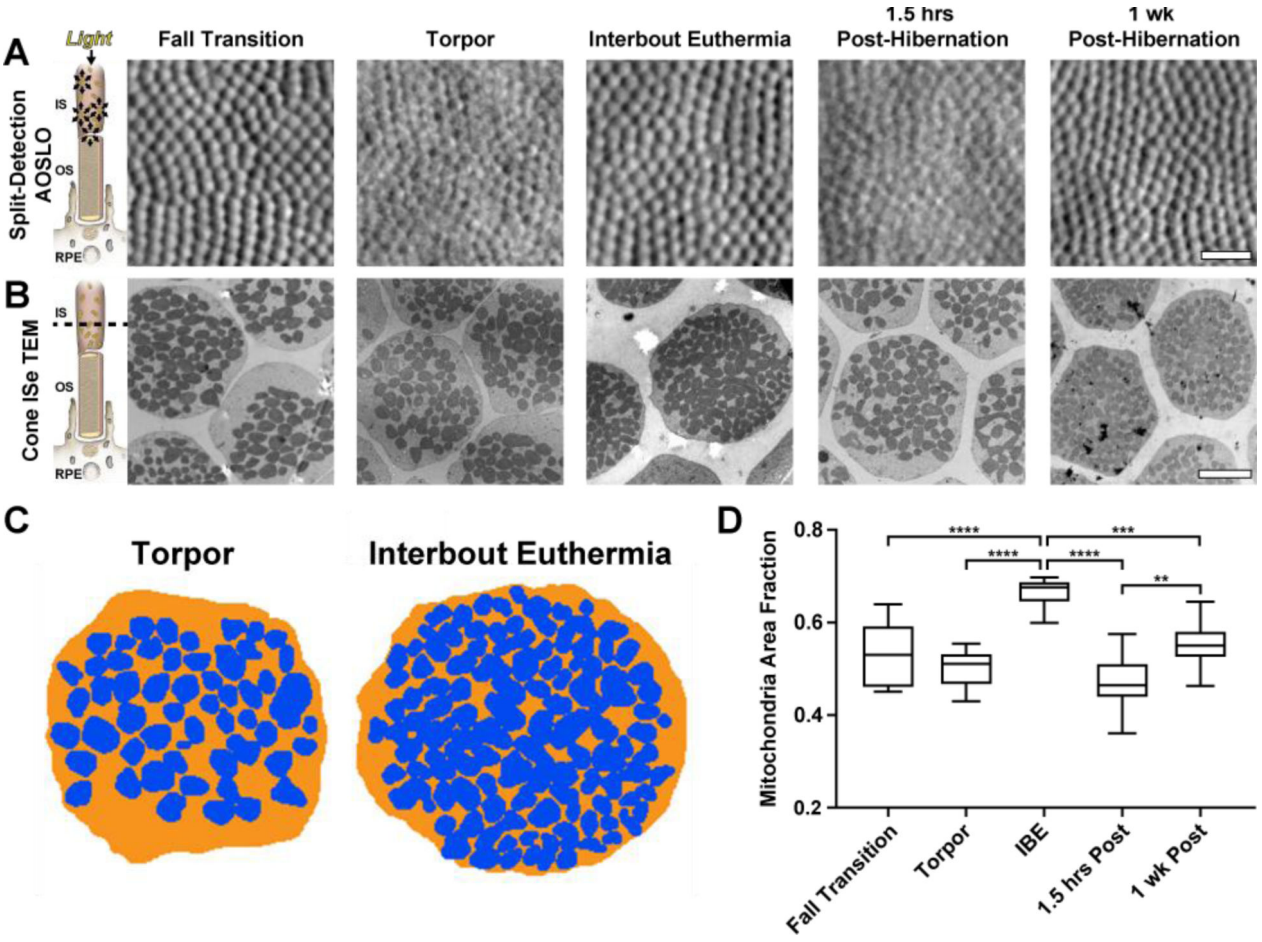

Figure 5 –.

Intra-animal comparisons of split-detection AOSLO (A) and transverse TEM inner segment ellipsoid (ISe) sections (B). Photoreceptor schematic in (A) illustrates the hypothesized sources of split-detection AOSLO signal (Scoles et al., 2014), whereas the schematic in (B) shows the photoreceptor plane visualized with TEM (dashed line). Photoreceptor mitochondria were sparser in fall transition, torpor, and 1.5 hours post hibernation, compared to interbout euthermia (IBE) and 1-week post-hibernation. Residual photoreceptor structure was detected in all seasonal states via split-detection AOSLO (A). Mitochondrial packing within the ISe does not have a noticeable effect on the split-detection AOSLO image (A & B). Representative torpor and IBE mitochondrial volume segmentations (blue) within the ISe (orange) are shown in (C). Box-and-whisker plots of mitochondria area fraction (mitochondria area ÷ ISe area) in 5 distinct physiological states are shown in (D). Boxes show median and interquartile ranges, *whiskers* show maximum and minimum values. IBE mitochondrial area fraction was significantly increased compared to all other physiological states, suggesting increased mitochondria recruitment during these brief periods of euthermia (D). $^{**}P < 0.01$; $^{***}P < 0.001$; $^{****}P < 0.0001$, one-way ANOVA. AOSLO scale bar = 20 μm. TEM scale bar = 2 μm.

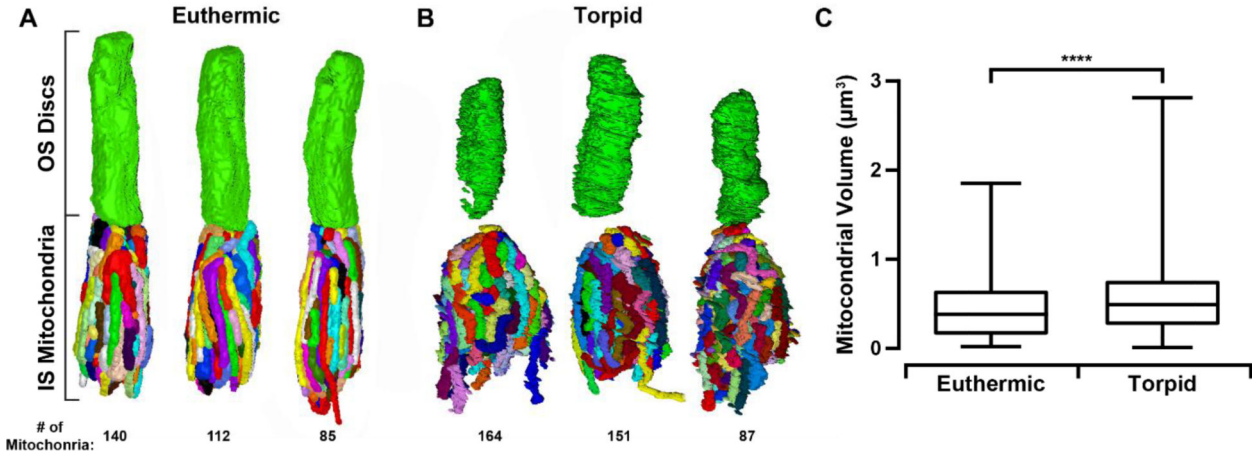

Figure 6 –.

3D volume reconstructions of cones from euthermic (A) and torpid (B) 13-LGS. The euthermic 13-LGS was sectioned with photoreceptors aligned vertically (A), and the torpid 13-LGS retina was sectioned with photoreceptors aligned horizontally (B). (C) Box-and-whisker plots of mitochondrial volumes from the 6 cells in (A) and (B) show a significant increase in the volume of torpid mitochondria (****$P < 0.0001$, Mann-Whitney test). *Boxes* show median and interquartile ranges, *whiskers* show maximum and minimum values.